

A possible determination of the quark radiation length in cold nuclear matter

R. B. Neufeld^{1,*}, Ivan Vitev^{1,†} and Ben-Wei Zhang^{2,1‡}

¹ *Los Alamos National Laboratory, Theoretical Division, Los Alamos, NM 87545, USA and*

² *Key Laboratory of Quark & Lepton Physics (Huazhong Normal University), Ministry of Education, China*

We calculate the differential Drell-Yan production cross section in proton-nucleus collisions by including both next-to-leading order perturbative effects and effects of the nuclear medium. We demonstrate that dilepton production in fixed target experiments is an excellent tool to study initial-state parton energy loss in large nuclei and to accurately determine the stopping power of cold nuclear matter. We provide theoretical predictions for the attenuation of the Drell-Yan cross section at large values of Feynman x_F and show that for low proton beam energies experimental measurements at Fermilab's E906 can clearly distinguish between nuclear shadowing and energy loss effects. If confirmed by data, our results may help determine the quark radiation length in cold nuclear matter $X_0 \sim 10^{-13}$ m.

PACS numbers: 25.75.Cj; 12.38.Bx; 24.85.+p

I. INTRODUCTION

The energy loss of a charged particle as it traverses dense matter is a fundamental probe of the matter properties. Accurate theoretical calculations and experimental measurements of this quantity became one of the great early successes of the classical and quantum theories of electromagnetic interactions [1]. The stopping power, dE/dx , in the limit of large energies is dominated by bremsstrahlung processes and is related to the radiation length, X_0 , of charged particles in matter as follows:

$$-dE/dx = E/X_0. \quad (1)$$

In Eq. (1) X_0 is approximately independent of the incident particle momentum. Precise knowledge of the stopping power and radiation length of materials is widely used today in X-ray tomography, muon and proton radiography, and high energy nuclear and particle physics detector development and instrumentation.

The fundamental constituents of nuclei, quarks and gluons, predominantly interact via their color charge. The forces between them are described from first principles by the theory of strong interactions, Quantum Chromodynamics (QCD), and are much larger in magnitude than the electromagnetic force. In the last decade, advances in high energy many-body QCD have enabled exploration of parton energy loss [2–5] in a novel hot and dense state of nuclear matter - the quark-gluon plasma (QGP). The predicted suppression of energetic particle production in nucleus-nucleus (A+A) collisions, dubbed jet quenching, is now definitively established [6, 7].

Alongside the excitement of this new discovery comes the realization that one of the biggest gaps in our current knowledge of nuclear reactions in extremis is the stopping power of cold nuclei for color-charged particles. In d+Au collisions at the Relativistic Heavy Ion Collider (RHIC), where the QGP is not formed, a similarly large suppression of particle production at large forward rapidity is observed [8, 9]. STAR experimental data on π^0 attenuation at $y = 4$, for example, can be fitted with disparate models that emphasize either large shadowing or large nuclear stopping. A more realistic calculation that includes the Cronin effect [10], high-twist shadowing [11], and initial-state energy loss [12] - all independently constrained in different processes and center of mass energies - is presented in Figure 1. The incorporation of these effects in the perturbative QCD calculation is briefly summarized in Ref. [13]. Our new results show that both coherent and inelastic scattering on the nucleus have comparable impact on the observed cross section attenuation in this kinematic range. This finding stresses once again the need to identify and reliably evaluate experimental observables that are clean and sensitive signatures of jet energy loss in cold nuclear matter.

From a phenomenological point of view, the significance of cold nuclear matter energy loss is well-established [14–17]. Theoretically, until recently, only final-state inelastic interactions in large nuclei relevant to semi-inclusive deeply inelastic scattering have been considered [18]. A new comparative study of initial-state and final-state energy loss [12] suggests that in the limit of large parton energies these exhibit strikingly different path length and parent parton energy dependencies:

$$\Delta E_{\text{initial-state}}^{\text{rad.}} \sim \kappa_{LPM} C_R \alpha_s E \frac{L}{\lambda_g}, \quad (2)$$

$$\Delta E_{\text{final-state}}^{\text{rad.}} \sim C_R \alpha_s \frac{\xi^2 L^2}{\lambda_g}. \quad (3)$$

*Electronic address: neufeld@lanl.gov

†Electronic address: ivitev@lanl.gov

‡Electronic address: bwzhang@iopp.cnu.edu.cn

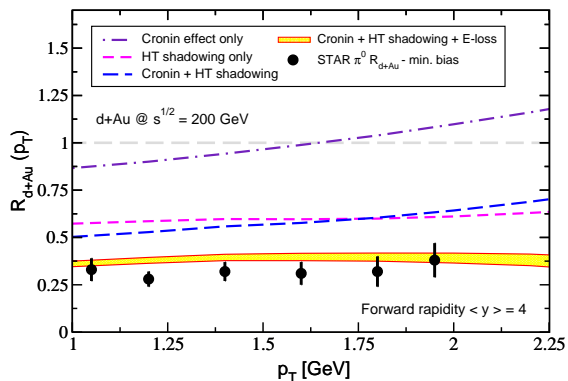


FIG. 1: Neutral pion suppression in minimum bias d+Au collisions at $y = 4$ at RHIC. Theoretical calculations that include known nuclear matter effects are shown. A complete simulation gives a good description of the experimental data.

Here, C_R is the quadratic Casimir in the fundamental and adjoint representations for quarks and gluons, respectively, λ_g is the gluon mean free path of $\mathcal{O}(1 \text{ fm})$ and α_s is the strong coupling constant. In this paper we refer to the soft interactions with typical transverse momentum transfers squared $\xi^2 \sim 0.1 \text{ GeV}^2$ for quarks prior to the large Q^2 scattering as initial-state. Similarly, the soft interactions after the hard scattering are described as final-state. We emphasize that such separation is only possible if $\xi^2 A^{1/3} \ll Q^2$. We will only be interested in lepton pair production of invariant mass squared $M^2 = Q^2 \geq 10 \text{ GeV}^2$, which is compatible with this constraint. Finally, we point out that the ξ^2 dependence in Eq. (2) is implicit through κ_{LPM} , the overall suppression factor relative to the incoherent Bertsh-Gunion bremsstrahlung.

The differential medium-induced bremsstrahlung spectrum can be expressed as a solution of an inhomogeneous recurrence relation with suitably chosen boundary conditions [12]. These boundary conditions differ for initial-state and final-state energy loss and the results will be correspondingly different. Final-state interactions and Eq. (3) have been investigated in detail, for example see [2–5]. Let us now focus on Eq. (2). Our starting point is the integral form for the double differential medium-induced gluon bremsstrahlung spectrum [12]:

$$k^+ \frac{dN^g(IS)}{dk^+ d^2\mathbf{k}} = \frac{C_R \alpha_s}{\pi^2} \int d^2\mathbf{q} \frac{\xi_{\text{eff}}^2}{\pi(\mathbf{q}^2 + \xi^2)^2} \left[\frac{L}{\lambda_g} \frac{\mathbf{q}^2}{\mathbf{k}^2(\mathbf{k} - \mathbf{q})^2} - 2 \frac{\mathbf{q}^2 - \mathbf{k} \cdot \mathbf{q}}{\mathbf{k}^2(\mathbf{k} - \mathbf{q})^2} \frac{k^+}{k^2 \lambda_g} \sin\left(\frac{\mathbf{k}^2 L}{k^+}\right) \right], \quad (4)$$

In Eq. (4) \mathbf{k} is the transverse momentum of the gluon relative to the direction of the parent parton, k^+ is its large lightcone momentum and \mathbf{q} is the momentum transfer from the nuclear medium. The formation time of the gluon $\tau_f = k^+/\mathbf{k}^2$ in comparison to the size of the medium L determines the degree of the destructive interference between the Bertsh-Gunion radiation and

the radiation from the hard scattering. Let us focus on $k^+ \sim E^+$ and recognize that when $\tau_f \ll L$ and \mathbf{k} varies, the phase factor $\sin(L/\tau_f)$ oscillates rapidly and averages to zero. One is left with the first term in the integrand of Eq. (4), which is the incoherent medium-induced bremsstrahlung:

$$\Delta E_{\text{initial-state}}^{\text{rad.}} \Big|_{\frac{E^+}{\mathbf{k}^2} \ll L} = \frac{C_R \alpha_s}{\pi^2} \frac{L}{\lambda_g} E \left\{ \int d^2\mathbf{k} \int d^2\mathbf{q} \times \frac{\xi_{\text{eff}}^2}{\pi(\mathbf{q}^2 + \xi^2)^2} \frac{\mathbf{q}^2}{\mathbf{k}^2(\mathbf{k} - \mathbf{q})^2} \right\}. \quad (5)$$

In the opposite limit $\tau_f \gg L$ for $k^+ \sim E^+$ we can expand the sine function to lowest order and obtain:

$$\Delta E_{\text{initial-state}}^{\text{rad.}} \Big|_{\frac{E^+}{\mathbf{k}^2} \gg L} = \frac{C_R \alpha_s}{\pi^2} \frac{L}{\lambda_g} E \left\{ \int d^2\mathbf{k} \int d^2\mathbf{q} \frac{\xi_{\text{eff}}^2}{\pi(\mathbf{q}^2 + \xi^2)^2} \left[\frac{1}{(\mathbf{k} - \mathbf{q})^2} - \frac{1}{\mathbf{k}^2} \right] \right\}. \quad (6)$$

Note that the overall multiplicative coefficients $\{\dots\}$ in Eqs. (5) and (6) have to be evaluated numerically with the relevant kinematic cuts specified in Ref. [12]. In the coherent regime the coefficient also reflects the destructive interference effect between the bremsstrahlung associated with the soft scattering and the bremsstrahlung associated with the large Q^2 process and can be numerically small. As the energy of the parent parton in the rest frame of the large nucleus grows, the approximation for $\Delta E_{\text{initial-state}}^{\text{rad.}}$ given by Eq. (6) becomes more relevant. This is the basis for the advocated energy and path length dependence in Eq. (2).

Of course, there are always parts of the emitted gluon phase space (k^+, \mathbf{k}) that are not compatible with simple approximations. For this reason, we first evaluate the fully differential bremsstrahlung spectrum numerically from Eq. (4), as described in [12]. From Eq. (1) in the small energy loss limit we can then quote a radiation length:

$$X_0 = LE \left[\int dk^+ \int d^2\mathbf{k} k^+ \frac{dN^g(E, L)}{dk^+ d^2\mathbf{k}} \right]^{-1}. \quad (7)$$

To summarize, for final-state interactions, the destructive Landau-Pomeranchuk-Migdal (LPM) interference leads to a change in the functional form of radiative energy loss. Eq. (3) does not allow for a natural definition of a radiation length and implies that the experimentally observable effects are limited to relatively small quark and gluon energies. In contrast, even if the LPM suppression factor $\kappa_{LPM} \sim 1/10$ in Eq. (2), $\Delta E_{\text{initial-state}}^{\text{rad.}}$ retains some of the characteristics of incoherent bremsstrahlung, see Eqs. (4), (5) and (6). For this reason, initial-state energy loss can also significantly affect experimental observables in heavy ion collider experiments of much higher $\sqrt{s_{NN}}$ [13, 19, 20]. Furthermore, Eq. (2) implies that the stopping power of cold nuclear matter for partons prior to a hard $Q^2 \gg \Lambda_{QCD}^2$ scattering can be characterized by a radiation length X_0 defined

in Eq. (7). One can see parametrically from Eq. (2) that X_0 is expected to be of $\mathcal{O}(10 \text{ fm} - 100 \text{ fm})$ - the shortest radiation length in nature, ten orders of magnitude smaller than the radiation length of high- Z materials, such as tungsten, for electrons.

The Drell-Yan process in heavy ion collisions [47] - $q + \bar{q} \rightarrow \gamma^* \rightarrow l^+ + l^-$ at lowest order (LO) - is an ideal probe of initial-state effects. The final-state particles do not interact strongly with the nuclear medium, providing a relatively clean experimental signature. Still, definitive separation of leading-twist shadowing effects [21–23] and parton energy loss [12, 24–27] has so far proven challenging [28, 29]. In no small part this difficulty arises from the fact that the very same Drell-Yan data in proton-nucleus (p+A) reactions is used to constrain the shadowing parameterizations [30]. Going to higher center of mass energies, such as what is available at RHIC and the Large Hadron Collider (LHC), will only amplify this unfortunate ambiguity. In this paper we demonstrate how dilepton production in conjunction with a suitably low proton beam energy $E_{\text{beam}} = 120 \text{ GeV}$, corresponding to $\sqrt{s_{NN}} = 15 \text{ GeV}$, at Fermilab's experiment E906 can disentangle initial-state energy loss and nuclear shadowing effects and pinpoint the stopping power of cold nuclear matter for quarks and gluons with $\sim 20\%$ accuracy.

Our work is organized as follows. In Section II we investigate lepton pair production in hadron-hadron reactions at next-to-leading order (NLO) in collinear factorized perturbative QCD and validate the theoretical simulation tools against experimental data. In Section III we discuss the cold nuclear matter (CNM) effects: initial-state energy loss and nuclear shadowing. A complete calculation of the dilepton production rate in p+A collisions at NLO that includes CNM effects is given in Section IV. We compare results to existing data on the attenuation of the Drell-Yan cross section in reactions with nuclei and present predictions for this suppression versus the cold nuclear matter radiation length X_0 for the upcoming E906 measurements. A summary and conclusions are presented in Section V.

II. THE DRELL-YAN PROCESS IN P+P COLLISIONS

In this paper we will be interested in the differential Drell-Yan production cross sections $d\sigma^{DY}/dx_F dQ^2$ and $d\sigma^{DY}/dy dQ^2$ where $Q^2 = q^2 = (p_{l^+} + p_{l^-})^2$ is the invariant mass squared, $x_F = 2q_L/\sqrt{s}$ is the Feynman x_F , and $y = \frac{1}{2} \ln[(q_0 + q_L)/(q_0 - q_L)]$ is the rapidity of the lepton pair. For illustration, we start the discussion with the LO cross section in the collinear factorization approach [31]:

$$\frac{d\sigma^{DY}}{dx_F dQ^2} = \sum_{q, \bar{q}} \frac{4\pi e_q^2 \alpha^2}{9Q^2 s(x_1 + x_2)} f_{q(\bar{q})}(x_1, \mu) f_{\bar{q}(q)}(x_2, \mu). \quad (8)$$

In Eq. (8) $\alpha \approx 1/137$, e_q is the quark fractional electric charge and $f_i(x_i, \mu)$ are the parton distribution functions.

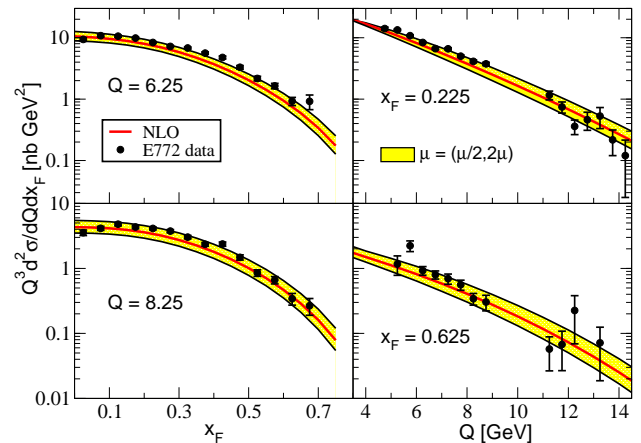


FIG. 2: Next-to-leading order calculations for the muon pair production cross section in p+D collisions at $\sqrt{s_{NN}} = 38.8 \text{ GeV}$ is compared to Fermilab E772 experimental data. The yellow bands represent the theoretical uncertainty due to choice of factorization and renormalization scales. We have only included isospin effects for the deuterium target.

The incident parton lightcone momentum fractions x_1, x_2 obey the relations:

$$x_1 x_2 = Q^2/s, \quad x_F = x_1 - x_2. \quad (9)$$

It is well-known that the perturbative next-to-leading order corrections to the Drell-Yan process can be quite significant [32–34]. The NLO calculation also adds a Compton scattering contribution to the annihilation graphs. Schematically, the one-loop cross section can be written as:

$$\frac{d\sigma_{NLO}^{DY}}{dQ^2 dx_F} = \frac{d\sigma_A^{DY}}{dQ^2 dx_F} + \frac{d\sigma_C^{DY}}{dQ^2 dx_F}. \quad (10)$$

The importance of going to $\mathcal{O}(\alpha^2 \alpha_s)$ is two-fold. First, it removes phenomenological K_{NLO} factors and allows a more reliable evaluation of the perturbative uncertainty through the variation of the renormalization and factorization scales $\mu_R = \mu_f = \mu$. Second, it facilitates a more accurate incorporation of dynamical nuclear effects that scale with the quadratic Casimir, which plays the role of the average squared color charge for quarks and gluons. In this work we implement the NLO Drell-Yan cross section calculation following Ref. [33].

An alternative approach to lepton pair production is based on the dipole model [35, 36]. In this model the Drell-Yan process is viewed as induced virtual photon bremsstrahlung in the target rest frame and nuclear effects are parameterized in the dipole cross section. In this paper we adhere to the traditional QCD factorization approach where higher-order corrections can be systematically evaluated order-by-order in perturbation theory. Furthermore, nuclear effects in perturbative QCD are incorporated at the cross section level as opposed to the amplitude level and are thus dependent on the average path length of partons through dense matter [48].

To test the baseline perturbative calculation for the Drell-Yan production cross section we compare our simulation results to Fermilab E772 data [37] from a fixed deuterium target experiment with an incident proton beam energy $E_{\text{beam}} = 800$ GeV in Figure 2. We take into account isospin effects as described in [38]. The left panels of Figure 2 show results for two different values of the lepton pair mass Q . The right panels show results for two different values of x_F . The yellow band represents the perturbative uncertainty due to the variation of the renormalization and factorization scales $Q/2 \leq \mu \leq 2Q$. We have checked that shadowing or energy loss effects for the deuterium target have less than a few % effect on the calculated cross section and are not shown in Figure 2 for simplicity.

III. COLD NUCLEAR MATTER EFFECTS

As seen in Figure 1, cold nuclear matter effects can significantly alter the production cross section for energetic/massive final states. Universal initial-state leading-twist shadowing effects are incorporated in nuclear parton distributions (nPDFs). Application for different observables or different $\sqrt{s_{NN}}$ is achieved by multiplying the standard parton distribution functions (PDFs) with a nPDF correction factor [38]. Alternatively, one can attempt to calculate CNM effects associated with the elastic, inelastic and coherent initial-state and final-state parton interactions in large nuclei from first principles [41]. This latter approach aims to elucidate the physics that underlays the observed nuclear modification. To date, there is no global nPDF analysis that attempts to separate the process-dependent and process-independent effects, largely due to the limited knowledge of the latter. Better theoretical and experimental control on cold nuclear matter energy loss is one step to help rectify this deficiency.

The process-dependent nuclear effects in question are enumerated below. First comes the Cronin effect that is often modeled through initial-state transverse momentum broadening [42] and affects the q_T distributions of energetic particles. In this manuscript we consider q_T -integrated cross sections, see for example Eqs. (8) and (10), and do not include the Cronin effect. Next comes dynamical shadowing that arises from the coherent final-state interactions of the recoil parton in the nuclear target [11]. For the Drell-Yan process at LO this effect vanishes since there is no parton in the final state. At NLO there is indeed a parton in the final state, however, for the dilepton masses of interest $Q = 4 - 10$ GeV the power suppressed high-twist shadowing effects, $\propto (A^{1/3}\xi^2)/Q^2$ where $\xi^2 \sim 0.1$ GeV², are expected to be negligible. This leaves the stopping power of large nuclei for incoming quarks and gluons as the most significant dynamical nuclear effect for Drell-Yan production. We discuss the cold nuclear matter energy loss below since it is central to our paper.

We evaluate initial-state energy loss numerically for minimum bias p+A reactions with deuterium (²D), beryllium (⁹Be), carbon (¹²C), aluminum (²⁷Al), iron (⁵⁶Fe), and tungsten (¹⁸⁴W) targets following Ref. [12]. We use $\lambda_g = 1$ fm for the gluon mean free path and vary the momentum transfer per interaction with the medium from $\xi = 0.175$ GeV to $\xi = 0.5$ GeV [49]. Comparing our results to Eq. (7) we find that in the limit of small energy loss $\Delta E_{\text{initial-state}}^{\text{rad}} \ll E$ or, equivalently, $L \ll X_0$, the radiation length of 100 GeV quarks in cold nuclear matter is between 30 fm and 160 fm for the parameters discussed above. We also calculate the probability distribution $P_{q,g}(\epsilon)$ for quarks and gluons to lose a fraction of their energy $\epsilon = \sum_i \omega_i/E$ due to multiple gluon emission in the Poisson approximation [38, 39]:

$$\int_0^1 P_{q,g}(\epsilon) d\epsilon = 1, \quad (11)$$

$$\int_0^1 P_{q,g}(\epsilon) \epsilon d\epsilon = \frac{\Delta E_{q,g}^{\text{rad. initial-state}}}{E}. \quad (12)$$

The calculation and/or implementation of initial-state or final-state energy loss processes focuses on real medium-induced gluon emission. Let us consider definitiveness the energy loss of the first incoming parton (characterized by lightcone momentum p_1^+ and fraction x_1). The differential distribution of emitted gluons itself is evaluated by separating it from the partonic scattering cross section. For a general hard process:

$$\frac{d\sigma}{dPS} = \int dx_1 dx_2 f(x_1) f(x_2) \int d\epsilon \frac{\langle |M[p_1^+(1-\epsilon), p_2^+]|^2 \rangle}{2x_1(1-\epsilon)x_2s} \times (2\pi)^4 \delta^4(p_i - p_f) \frac{dN^g(\epsilon)}{d\epsilon}. \quad (13)$$

In Eq. (13) $\epsilon = k^+/p_1^+$ and parton flavor indices and the sum over flavors are not shown explicitly. We emphasize that the energy loss results only depend on the details of the final state through the value of p_1^+ and in the δ -function $p_i = p_1(1-\epsilon) + p_2$. We have also integrated over the gluon's transverse momentum \mathbf{k} , noting that the direction of the incoming parton does not change on average. In the soft gluon approximation, which we use in this study, medium-induced bremsstrahlung can be identified even at the amplitude level [3, 12]. Proper factorization of the differential energy loss distribution in the $\epsilon \rightarrow 1$ limit can only be shown in QCD at the cross section level [40]. This distribution does include the interference of the bremsstrahlung from the soft in-medium scattering with the bremsstrahlung from the large Q^2 process.

For a single ($n_g = 1$) emitted gluon $dN^g(\epsilon)/d\epsilon = P(\epsilon)$ is also the probability distribution for fractional energy loss ϵ . In general, $n_g \neq 1$ and the probability distributions $P_{q,g}(\epsilon)$, see Eqs. (11) and (12), is constricted from $dN^g(\epsilon)/d\epsilon$ in the independent Poisson approximation [38, 39] to gluon emission. Changing variables, $x_1 \rightarrow x_1/(1-\epsilon)$, and the order of the integration we

find:

$$\frac{d\sigma}{dPS} = \int dx_1 dx_2 \left[\int d\epsilon P(\epsilon) f\left(\frac{x_1}{1-\epsilon}\right) \right] f(x_2) \times \frac{1}{2x_1 x_2 s} \langle |M[p_1^+, p_2^+]|^2 \rangle (2\pi)^4 \delta^4(p_i - p_f). \quad (14)$$

From Eq. (14), initial-state energy loss is most conveniently implemented in the perturbative calculations of the differential Drell-Yan cross section Eqs. (8) and (10) as follows:

$$f_{q,\bar{q}}(x, \mu) \rightarrow \int_0^1 d\epsilon P_q(\epsilon) f_{q,\bar{q}}\left(\frac{x}{1-\epsilon}, \mu\right), \quad (15)$$

$$f_g(x, \mu) \rightarrow \int_0^1 d\epsilon P_g(\epsilon) f_g\left(\frac{x}{1-\epsilon}, \mu\right). \quad (16)$$

Here, $f(x, \mu)$ is the distribution function of the parton from the incident proton. The physical meaning of Eqs. (15) and (16) is that in the presence of nuclear stopping larger quark and gluon energies in the nuclear wave function are probed by the same lepton pair kinematics. These results imply that the attenuation of the Drell-Yan cross section depends not only on the magnitude of cold nuclear matter energy loss but also on the steepness of the PDFs. Specifically, large suppression is expected at large values of Feynman x_F (or large rapidity) where $f'(x, \mu) \ll 0$. We have denoted by $f'(x, \mu)$ the derivative of the parton distribution function with respect to the momentum fraction x . Finally, we note that accounting for fluctuations in the energy loss via $P_{q,g}(\epsilon)$ is critical when jet and particle production is near kinematic limits. We have checked that using the mean energy loss $\Delta E_{q,g}^{\text{rad. initial-state}}/E$, instead of the full convolution over $P_{q,g}(\epsilon)$, overpredicts the suppression at large x_F by more than a factor of two.

IV. LEPTON PAIR PRODUCTION IN P+A COLLISIONS

We now present results from the full calculation of Drell-Yan production at NLO that include cold nuclear matter effects. We first consider existing measurements from the Fermilab E772/E886 experiment [16] which were performed using several nuclear targets in the path of a proton beam of energy $E_{\text{lab}} = 800$ GeV. Dilepton data and theoretical simulations are presented in Figure 3 as the ratio of the differential cross sections on two different targets in minimum bias p+A reactions scaled down to a binary nucleon-nucleon interaction:

$$\text{Ratio}(A/B) \equiv R_{AB}^{DY} = B \cdot \frac{d\sigma_{pA}^{DY}}{dx_F dQ^2} / A \cdot \frac{d\sigma_{pB}^{DY}}{dx_F dQ^2}. \quad (17)$$

We considered two different invariant mass ranges $4 \text{ GeV} < Q < 5 \text{ GeV}$ (left panels) and $6 \text{ GeV} < Q < 7 \text{ GeV}$ (right panels). We also included two different ratios: R_{WD}^{DY} and R_{WBe}^{DY} in the top and bottom panels,

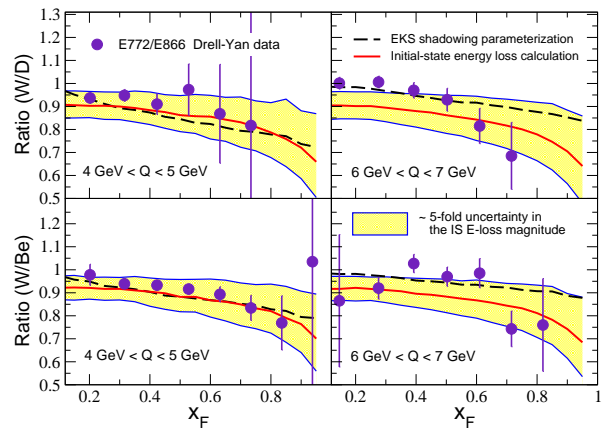


FIG. 3: Plot of the ratio of the dimuon cross section $\sigma(p+W)/\sigma(p+A)$, where $A = D, Be$, from both experiment and theory for 800 GeV protons colliding with a fixed nuclear target. The theory curves are the NLO Drell-Yan cross section calculation, including shadowing effects and initial-state energy loss, respectively. The yellow bands indicate a five-fold variation of the mean quark medium-induced energy loss.

respectively. The dashed lines represent a calculation of the cross section ratios that incorporates a leading twist-shadowing parameterization [30]. The solid lines show our simulation with initial-state energy loss [12] that is compatible with the theoretical description of RHIC d+A and A+A data [13, 19, 20].

It should be noted that while both calculations describe the E772/E866 data with equal acumen, they emphasize completely different physics. The former simulation assumes a modification of the nuclear wave-function and is driven by the decreasing momentum fraction x_2 of the parton in the nucleus when Feynman x_F grows. The behavior of R_{AB}^{DY} for the latter case is governed by the energy loss of the incident parton that carries an increasing fraction x_1 of the momentum of the proton. The current accuracy of the experimental data does not allow one to distinguish between these two competing paradigms. Furthermore, it cannot precisely constrain the magnitude of $\Delta E_{\text{initial-state}}^{\text{rad.}}$. The yellow band in Figure 3 represents a variation of the typical momentum transfers between the incoming parton and the medium ξ in the range of 0.175 GeV to 0.5 GeV, as described in Section III. Such variation induces an approximately five-fold uncertainty in the magnitude of the stopping power of large nuclei for incident partons. While the extreme cases of very large or very small energy loss are not favored by the data, a considerable uncertainty can still exist for this physics scenario.

A unique opportunity to disentangle initial-state energy loss effects from nuclear shadowing is presented by the approved and now under construction Fermilab experiment E906 [43, 44]. It is a fixed target Drell-Yan experiment with $E_{\text{beam}} = 120$ GeV. Its primary goal is to accurately measure the large x_F \bar{d}/\bar{u} asymmetry and it can comfortably cover the $0.4 \leq x_F \leq 0.9$ and

$M_{J/\psi} \leq Q \leq M_T$ kinematic range. A secondary goal of E906 is to precisely determine cold nuclear matter energy loss. Its low center of mass energy per nucleon pair $\sqrt{s_{NN}} = 15$ GeV allows a selection of the dilepton mass which practically eliminates shadowing effects. In contrast, nuclear stopping is expected to be even more important at these energies.

Next, let us review again the prerequisites for the determination of the stopping power of cold nuclear matter and its radiation length X_0 . First, one needs to identify the part of phase space where shadowing effects are minimal (we are interested specifically in the Drell-Yan process). Second, experimental measurements must establish a statistically significant suppression of the dilepton production cross section in p+A reactions $R_{pA}^{DY} < 1$ at large x_F . Third, one has to confirm an approximately linear dependence of R_{pA}^{DY} on the nuclear size $A^{1/3}$. Note that the $A^{1/3}$ dependence of the ΔE^{rad} is correlated with a linear dependence on the parton energy. This will allow for a proper extraction of X_0 .

Our numerical results, relevant to the E906 program, are presented in Figure 4. We have chosen to consider $d\sigma^{DY}/dx_F dQ^2$ versus Feynman x_F for $Q = 4.5$ GeV, and have carried out simulations for deuterium, carbon, iron, and tungsten targets. In order to obtain the ratio defined in Eq. (17), we have normalized the nuclear cross sections to that of a D target which minimizes any trivial isospin dependence. In all cases, the effects of shadowing, which are shown with dashed lines in Figure 4, are negligible. On the other hand, energy loss effects, represented by solid lines for three different radiation lengths $X_0 = 30$ fm, 50 fm and 160 fm, can clearly be detected, especially for large values of x_F . We have also included in Figure 4 simulated experimental data which shows the anticipated E906 statistical precision for R_{WD}^{DY} [43]. With careful selection of the heavy nuclear targets, such as Fe and W, and the lepton pair kinematics, the two competing pictures for the physics that underlays the suppression of dilepton production in p+A reactions can be definitively confirmed or refuted. As seen in Figure 4, the radiation length of cold nuclear matter for quarks can likely be constrained with $\sim 20\%$ accuracy.

The bottom right panel in Figure 4 shows the attenuation of the Drell-Yan cross section at a fixed value of $x_F = 0.9$ versus the linear size $\sim A^{1/3}$ of the target nucleus. Our results reflect the fact that initial-state energy loss of quarks and gluons prior to a large Q^2 scattering depends approximately linearly on the path length through strongly interacting matter. This is in contrast to final-state energy loss where quadratic path-length dependence [2–4] would suggest $A^{2/3}$ scaling of the attenuation of the lepton pair production rate. E906 measurements will also help clarify this open question.

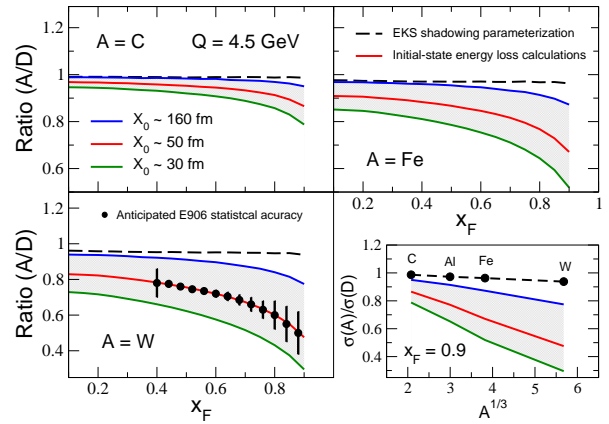


FIG. 4: Next-to-leading order theoretical predictions for the Drell-Yan dimuon cross section attenuation $\sigma(p+A)/\sigma(p+D)$ at Fermilab’s E906. As with Figure 3, the curves include shadowing effects (dashed line) or initial-state energy loss (solid lines), respectively. We have considered three different radiation lengths X_0 of quarks in large nuclei, ranging from 30 fm to 160 fm. The lower right panel highlights the difference between the two physics scenarios at large x_F as a function of $A^{1/3}$.

V. SUMMARY AND CONCLUSIONS

One of the most pressing current questions in the theory and phenomenology of heavy ion reactions at high energies is related to the stopping power of cold nuclear matter for energetic quarks and gluons. Plentiful experimental evidence and theoretical justification exist for the significance of initial-state energy loss effects [8, 9, 12, 13, 15–17, 19]. It is, therefore, unfortunate that attempts to precisely determine their strength have so far been inconclusive. These earlier studies employed a functional form for the energy loss that might have been better-suited to describe final-state scattering processes in the QGP, and yielded large uncertainties for $-dE/dx$ [16, 24, 25, 28]. Little is known quantitatively for the interactions of partons and hadrons in cold nuclear matter beyond the interaction lengths, or mean free paths, for selected few species, such as protons or alpha particles. Only recently have developments in the theory of quark and gluon propagation in cold nuclear matter suggested that initial-state energy loss in QCD retains certain characteristics of induced electromagnetic bremsstrahlung [12]. Thus, it can be described in terms of a radiation length X_0 . A real opportunity exists today to determine this shortest radiation length in nature.

To this end, we have embarked on a program to develop the theoretical tools that can both motivate and facilitate the upcoming E906 experimental p+A program. To ensure that the baseline differential Drell-Yan cross sections in elementary nucleon-nucleon reactions are reliably estimated, we opted for a next-to-leading order accuracy of the perturbative QCD calculation. The new simulation tool was validated against Fermilab’s

E772 muon pair production measurements in p+D reactions. Next, we implemented initial state-nuclear effects, such as leading-twist shadowing and medium-induced bremsstrahlung in large nuclei. Care was taken to incorporate the fluctuations in the magnitude of parton energy loss. We showed that neglect of these fluctuations will result in a severe overestimate of the attenuation of the lepton pair production rate. Results from our work have been used to evaluate the dilepton background for the Υ measurements at RHIC via the $l^+ + l^-$ decay channel [45].

For nuclear targets with large mass number we first verified that existing Drell-Yan measurements cannot distinguish between calculations that incorporate initial-state energy loss and leading-twist shadowing parametrizations. While this observation has been made before, our work is more general in that it goes beyond the fixed energy loss per unit length conjecture. Our results also suggest that moving to the higher center-of-mass energies of RHIC and the LHC will not help separate the two competing physics effects. We showed that radiation lengths in cold nuclear matter for quarks X_0 of the order of 50 fm to 100 fm are compatible with the $E_{\text{beam}} = 800$ GeV Fermilab E772/E866 data. The same stopping power of large nuclei has worked well for the theoretical description of hard probes production at RHIC.

To definitively confirm or refute initial-state energy loss as the principal nuclear effect which leads to the suppression of the Drell-Yan cross section in p+A reactions we presented predictions for the upcoming Fermilab experiment E906. We exploited its low center-of-mass energy to identify a kinematic region where shadowing

effects vanish. We demonstrated that, with the anticipated statistical accuracy of the data in the large x_F region, radiation lengths as large as 200 fm can be detected. If X_0 is of $\mathcal{O}(50 \text{ fm})$, there is a good chance that it can be determined with $\sim 20\%$ accuracy.

As a final note, we recognize that experimental measurements may differ from the most sophisticated theoretical predictions. With the next-to-leading order simulation tools at hand, upcoming E906 experimental data can be quickly and reliably analyzed for parton energy loss effects. The theoretical progress described here, combined with experimental advances in the use of dimuons, is expected to result in the first unambiguous measurement of quark energy loss in nuclei [46] and provide the much-needed standard candle for gauging the nuclear response to strongly interacting particles.

Acknowledgments

We thank M. Leitch and P. McGaughey for providing us with Fermilab E772/E866 experimental data. This research is supported by the US Department of Energy, Office of Science, under Contract No. DE-AC52-06NA25396 and in part by the LDRD program at LANL, by the Ministry of Education of China with the Program NCET-09-0411, by National Natural Science Foundation of China with Project No. 11075062, and CCNU with Project No. CCNU09A02001.

-
- [1] W. M. Yao *et al.* [Particle Data Group], J. Phys. G **33**, 1 (2006) Chapter 27;
- [2] R. Baier, Y. L. Dokshitzer, A. H. Mueller, S. Peigne and D. Schiff, Nucl. Phys. B **483**, 291 (1997) [arXiv:hep-ph/9607355].
- [3] M. Gyulassy, P. Levai and I. Vitev, Phys. Rev. Lett. **85**, 5535 (2000) [arXiv:nucl-th/0005032].
- [4] X. N. Wang and X. f. Guo, Nucl. Phys. A **696**, 788 (2001) [arXiv:hep-ph/0102230].
- [5] P. B. Arnold, G. D. Moore and L. G. Yaffe, JHEP **0206**, 030 (2002) [arXiv:hep-ph/0204343].
- [6] S. S. Adler *et al.* [PHENIX Collaboration], Phys. Rev. Lett. **91**, 072301 (2003) [arXiv:nucl-ex/0304022].
- [7] J. Adams *et al.* [STAR Collaboration], Phys. Rev. Lett. **91**, 172302 (2003) [arXiv:nucl-ex/0305015].
- [8] I. Arsene *et al.* [BRAHMS Collaboration], Phys. Rev. Lett. **93**, 242303 (2004) [arXiv:nucl-ex/0403005].
- [9] J. Adams *et al.* [STAR Collaboration], Phys. Rev. Lett. **97**, 152302 (2006) [arXiv:nucl-ex/0602011].
- [10] I. Vitev, Phys. Lett. B **562**, 36 (2003) [arXiv:nucl-th/0302002].
- [11] J. w. Qiu and I. Vitev, Phys. Lett. B **632**, 507 (2006) [arXiv:hep-ph/0405068].
- [12] I. Vitev, Phys. Rev. C **75**, 064906 (2007) [arXiv:hep-ph/0703002].
- [13] R. Sharma, I. Vitev and B. W. Zhang, Phys. Rev. C **80**, 054902 (2009) [arXiv:0904.0032 [hep-ph]].
- [14] R. Vogt, Phys. Rev. C **61**, 035203 (2000). [hep-ph/9907317].
- [15] S. Gavin and J. Milana, Phys. Rev. Lett. **68**, 1834 (1992).
- [16] M. B. Johnson *et al.* [FNAL E772 Collaboration], Phys. Rev. Lett. **86**, 4483 (2001) [arXiv:hep-ex/0010051].
- [17] B. Z. Kopeliovich, J. Nemchik, I. K. Potashnikova, M. B. Johnson and I. Schmidt, Phys. Rev. C **72**, 054606 (2005) [arXiv:hep-ph/0501260].
- [18] E. Wang and X. N. Wang, Phys. Rev. Lett. **89**, 162301 (2002) [arXiv:hep-ph/0202105].
- [19] I. Vitev and B. W. Zhang, Phys. Rev. Lett. **104**, 132001 (2010) [arXiv:0910.1090 [hep-ph]].
- [20] I. Vitev and B. W. Zhang, Phys. Lett. B **669**, 337 (2008) [arXiv:0804.3805 [hep-ph]].
- [21] M. Arneodo, Phys. Rept. **240**, 301 (1994).
- [22] M. Hirai, S. Kumano and T. H. Nagai, Phys. Rev. C **70**, 044905 (2004) [arXiv:hep-ph/0404093].
- [23] N. Armesto, J. Phys. G **32**, R367 (2006) [arXiv:hep-ph/0604108].
- [24] F. Arleo, Phys. Lett. B **532**, 231 (2002) [arXiv:hep-ph/0201066].

- [25] G. T. Garvey and J. C. Peng, Phys. Rev. Lett. **90**, 092302 (2003) [arXiv:hep-ph/0208145].
- [26] C. G. Duan, L. H. Song, L. J. Huo and G. L. Li, Eur. Phys. J. C **29**, 557 (2003) [arXiv:hep-ph/0405113].
- [27] H. M. Wang, X. J. Sun and B. A. Zhang, Phys. Scripta **75**, 651 (2007).
- [28] M. A. Vasilev *et al.* [FNAL E866 Collaboration and NuSea Collaboration], Phys. Rev. Lett. **83**, 2304 (1999) [arXiv:hep-ex/9906010].
- [29] M. B. Johnson *et al.*, Phys. Rev. C **65**, 025203 (2002) [arXiv:hep-ph/0105195].
- [30] K. J. Eskola, V. J. Kolhinen and C. A. Salgado, Eur. Phys. J. C **9**, 61 (1999) [arXiv:hep-ph/9807297].
- [31] J. C. Collins, D. E. Soper and G. Sterman, Adv. Ser. Direct. High Energy Phys. **5**, 1 (1988) [arXiv:hep-ph/0409313].
- [32] G. Altarelli, R. K. Ellis and G. Martinelli, Nucl. Phys. B **157**, 461 (1979).
- [33] J. Kubar, M. Le Bellac, J. L. Meunier and G. Plaut, Nucl. Phys. B **175**, 251 (1980).
- [34] W. J. Stirling and M. R. Whalley, J. Phys. G **19** (1993) D1.
- [35] J. Raufeisen, J. -C. Peng, G. C. Nayak, Phys. Rev. **D66**, 034024 (2002); references therein. [hep-ph/0204095].
- [36] M. A. Betemps, M. B. G. Ducati, M. V. T. Machado *et al.*, Phys. Rev. **D67**, 114008 (2003). [hep-ph/0303100].
- [37] P. L. McGaughey *et al.* [E772 Collaboration], Phys. Rev. D **50**, 3038 (1994) [Erratum-ibid. D **60**, 119903 (1999)].
- [38] I. Vitev, Phys. Lett. B **639**, 38 (2006) [arXiv:hep-ph/0603010].
- [39] R. Baier, Y. L. Dokshitzer, A. H. Mueller *et al.*, JHEP **0109**, 033 (2001). [hep-ph/0106347].
- [40] G. Ovanesyan and I. Vitev, JHEP **1106**, 080 (2011) [arXiv:1103.1074 [hep-ph]].
- [41] I. Vitev, J. T. Goldman, M. B. Johnson and J. W. Qiu, Phys. Rev. D **74**, 054010 (2006) [arXiv:hep-ph/0605200].
- [42] A. Accardi, arXiv:hep-ph/0212148.
- [43] P. E. Reimer, J. Phys. G **34**, S107 (2007) [arXiv:0704.3621 [nucl-ex]].
- [44] E906 home page: <http://www.phy.anl.gov/mep/SeaQuest/>
- [45] M. Leitch, private communication.
- [46] I. Vitev, M. Liu, P. McGaughey, “The first precise determination of quark energy loss in nuclei”, Los Alamos Laboratory Directed Research and Development project, 2008-2010.
- [47] In this paper we will use the term heavy ion collisions to describe both p+A and A+A hadronic reactions at relativistic energies
- [48] For example, in a picture of interfering virtual photon production amplitudes from distinct nucleon-nucleon scatterings the path length will be the average of the two path lengths.
- [49] The momentum transfer between the jet and the medium is often denoted by μ . We use ξ in this paper to indicate that the default value corresponds to the same dimensional scale used in dynamical shadowing calculations.